Research in Astronomy and Astrophysics, 24:061001 (6pp), 2024 June https://doi.org/10.1088/1674-4527/ad44f1

The First Ground-based White Light Lunar Polarization Imaging: A New Kind of FeO Observation on the Near Side of the Moon

Wei-Nan Wang[1,3], Jin-Song Ping[2,3], Ming-Yuan Wang[2], Wen-Zhao Zhang[4], Han-Lin Ye[5], Xing-Wei Han[1], and Song-Feng Kou[6]
[1] Changchun Observatory, National Astronomical Observatories, Chinese Academy of Sciences, Changchun 130117, China; wangwn@cho.ac.cn
[2] National Astronomical Observatories, Chinese Academy of Sciences, Beijing 100101, China; jsping@bao.ac.cn
[3] University of Chinese Academy of Sciences, Beijing 101408, China
[4] Astronomy Department, Beijing Normal University, Beijing 100875, China
[5] International Center for Climate and Environment Sciences, Institute of Atmospheric Physics, Chinese Academy of Sciences, Beijing 100029, China
[6] Nanjing Institute of Astronomical Optics and Technology, Chinese Academy of Sciences, Nanjing 210042, China
Received 2023 December 14; revised 2024 April 17; accepted 2024 April 24; published 2024 June 24

Abstract

Lunar optical polarization is a fascinating phenomenon that occurs when sunlight reflects off the surface of the Moon and becomes polarized. This study employs a novel split-focus plane polarimetric camera to conduct the initial white light polarimetric observations on the near side of the Moon. We obtained the linear degree of polarization (DOP) parameters of white light by observation from the eastern and western hemispheres of the Moon. The findings indicate that the white light polarization is lower in the lunar highland than in the lunar maria overall. Combining the analysis of lunar soil samples, we noticed and determined that the DOP parameters of white light demonstrate high consistency with iron oxide on the Moon. This study may serve as a new diagnostic tool for the Moon.

Key words: techniques: photometric – polarization – methods: observational – Moon

1. Introduction

Lunar scientific observation from Earth has been helping us uncover the features and evolution of the Moon, and understand the state of the lunar surface and interaction. Optical technique plays a key role in this study, where polarization imaging is used to estimate lunar regolith grain size (Dollfus & Titulaer 1971; Shkuratov 1981; Shkuratov & Opanasenko 1992; Jeong et al. 2015) and the refractive index of the lunar regolith (Fearnside et al. 2016). This classical polarimetric method and scientific target of the Umov effect have been adopted by a Korean lunar remote sensing orbiter (Sim et al. 2019). Based on this effect on the lunar surface, grain size detection has been the main scientific objective. Historically, Umov effect on asteroids and of the Moon have considered only geometric grain size, and neither material homogeneity of asteroids nor heterogeneity of the lunar surface has yet been taken into consideration.

Polarization of scattered natural sunlight from the Moon can provide new insight into the lunar surface. Optical polarization may be influenced by the heterogeneity of the lunar surface. Polarization remote sensing of geometric information systems has been successfully used to detect heterogeneous ground material. Based on this method, an uneven composition of the lunar surface may be found from ground polarimetric imaging observation. Generally, common technologies and methods of exploring lunar heterogeneous minerals and their main elements (Fe, Ti, and others) rely on imaging spectral data, both in situ sensing and remote sensing (Lucey et al. 1998; Gillis et al. 2003). The interior of lunar soil grains may contain more fundamental compositional information which can be retrieved from optical polarization imaging. Polarization, as another dimension of light or an electromagnetic wave, is related to the crystal or subcrustal lattice of minerals.

In geoscience remote sensing, the advantages of polarimetric observation technology have been widely recognized by Tyo et al. (2006). The polarization state can effectively distinguish the states of different materials or surfaces on Earth. So, in order to test this idea, we carried out lunar polarimetric observation and tried to investigate the possibility of detecting the lunar surface compositions.

2. Observations

In this work, we conduct the first visible white light polarimetric observations of the Moon using a Schmidt–Cassegrain telescope of 0.2 m aperture in Xinjiang, China. The imaging instrument, consisting of a new division for the focal plane polarization camera, is used. The full resolution of the polarization camera is 2460×2070, and it adopts a Sony IMX250 MZR polarization chip, as illustrated in Figure 1. The linearly polarized light can be represented by Stokes parameters, and its linear degree of polarization (DOP) P can be

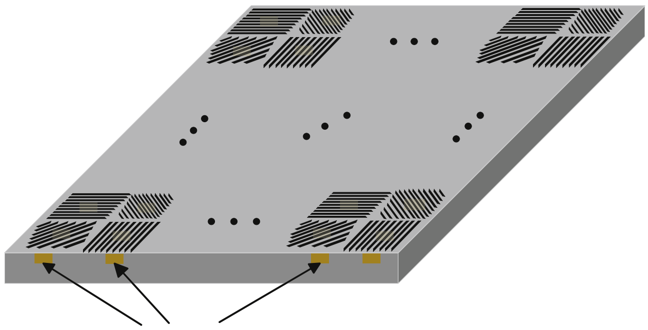

Figure 1. Block diagram of a division of focal plane polarimeter, cited by Powell & Gruev (2013).

expressed as

$$P = \frac{\sqrt{Q^2 + U^2}}{I}, \quad (1)$$

where Q, U and I are Stokes parameters. These are:

$$I = \frac{I_0 + I_{45} + I_{90} + I_{135}}{2}, \quad (2)$$

$$Q = I_0 - I_{90}, \quad (3)$$

$$U = I_{45} - I_{135}. \quad (4)$$

In the focal-plane polarimetric imaging method, each of the four (2×2) micropolarizer arrays with different polarization directions (0°, 45°, 90° and 135°) are obtained at the pixel level by inscribing different directional line grids on the photoreceptor chip. I_0, I_{45}, I_{90} and I_{135} represent the light intensity sub-images corresponding to the polarization directions of 0°, 45°, 90° and 135° of the polarizer, respectively. Each micropolarizer array corresponds to each pixel of the image sensor one by one. The focal-plane polarimetric imaging cannot acquire circular polarization. However, the circular polarization of the Moon (the fourth Stokes parameter) is negligibly small (Shkuratov et al. 2011).

The Stokes parameters are estimated using micropolarizer measurements from different locations in the focal plane array. The drawback is that the different instantaneous fields of view (IFOV) of neighboring pixels complicate the reconstruction process and are the primary source of false polarization signatures (Ratliff et al. 2009). The bicubic interpolation method is adopted to particularly improve the resolution reduction and the error of IFOV (Ratliff et al. 2009; Gao & Gruev 2011).

The instrument is calibrated by using the standard astronomical calibration method. All the Stokes parameters image data subtract bias, dark and flat-fielded auxiliary images by a data reduction pipeline running at the telescope. The bias and dark frames used in calibration are updated daily, and the flat fields are sufficiently stable only once. Moreover, relative calibration (Słowikowska et al. 2016; Ramaprakash et al. 2019) is performed by observing the polarization standard stars in the Heiles catalog (Heiles 2000) and the zero-bias standard stars taken from the Hubble Space Telescope atlas (Turnshek et al. 1990). These non-polarized standard stars are used to measure the instrumental polarization introduced by the telescope and instrument optics. These standard stars are generally imaged close to the array's center and can be used to correct the measured Stokes parameters before our lunar observations. The DOP images of the observed lunar surface is calculated using the Stokes parameters.

We observed the near-Earth side of the Moon during a period from August through 2022 October. On each night with clear weather, we obtained dozens of frames of the Moon for several minutes. The exposure time of each frame of the image is approximately 20–30 ms. We calibrated and mosaiced these frames from the same night into one image and chose the maximum white light DOP image by following Minsup Jeong et. (Jeong et al. 2015) methods from these images for both the western hemisphere and the eastern hemisphere. Moreover, we mosaiced the DOP maps of the eastern and western hemispheres to obtain the lunar nearside map, as shown in Figure 2.

3. Data

From the DOP map, we noticed that the white light polarization is higher in the lunar maria than highlands. In the region of Oceanus Procellarum, the white light polarization is maximum and the value is almost 20%. Besides the Umov effect, the DOP map may contain information about the lunar composition. Thus, we compared several images of ground mineral soil features with the polarization and noticed that the metal-oxygen compositions in Figure 2 were remarkably consistent with the DOP map. To investigate the correlation between the DOP parameters of visible white light on the lunar surface and the material composition of lunar soil, we retrieved the DOP of lunar sampling sites from Figure 2. Then we compared them with the corresponding metal abundances in the lunar soil samples.

These lunar sample data were acquired from Apollo, Luna, and China's Chang'E-5 (CE-5) missions, which are analyzed by Blewett et al. (Blewett et al. 1997) and Li et al. (2021). Totally 12 groups of data from ground samples are used in Table 1, with a remark about the iron oxide (FeO) values in calculations. Compositional data for lunar soils were compiled from data in the literature, and these values are for fine <1 mm sizes. Apollo missions 11, 12, and 14 as well as Luna missions 16, 20, and 24 collected samples are from individual points in small areas surrounding their respective landing sites. FeO value data given by literature are directly adopted for them. The lunar roving vehicle allowed Apollo 15, 16, and 17 to extend their range of surface operations. However, the lack of enough spatial resolution prevents distinguishing individual sampling

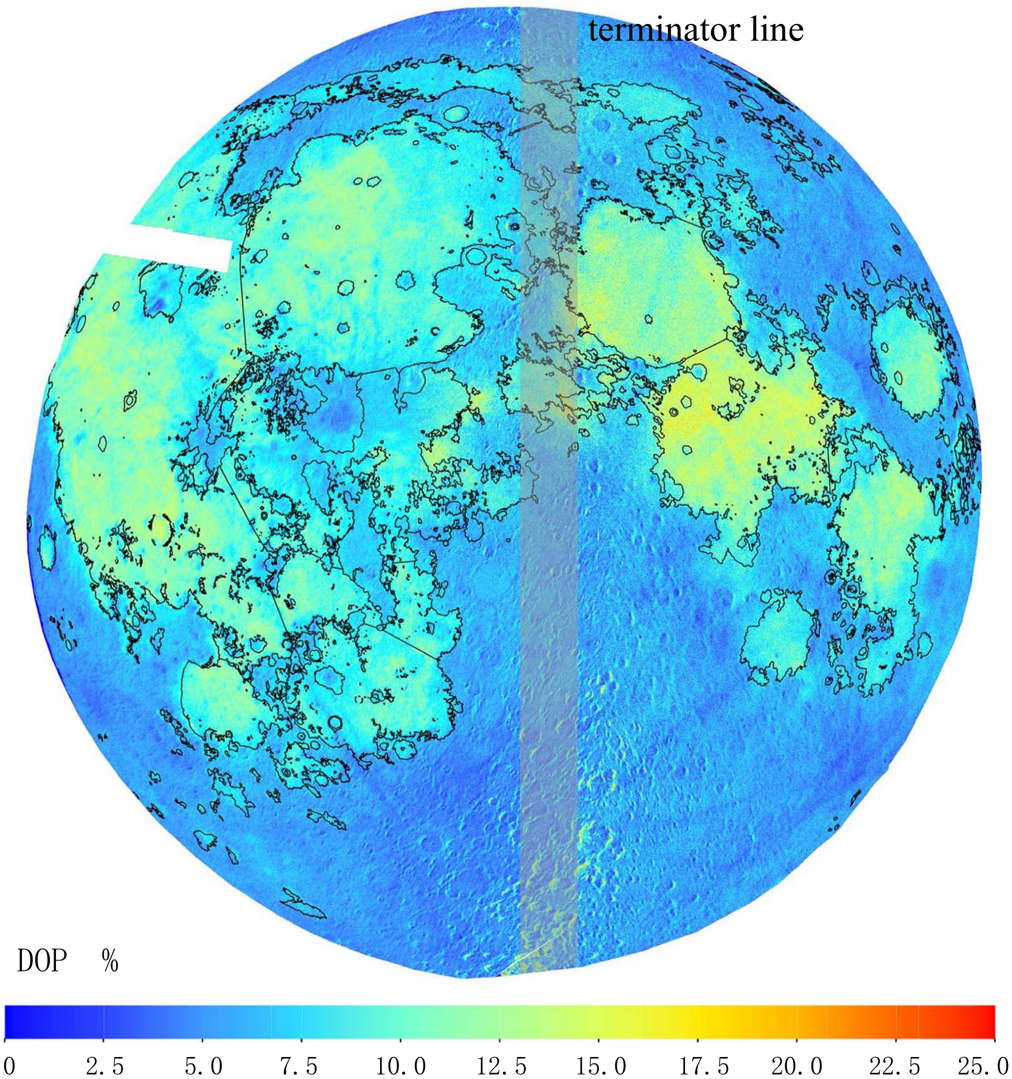

Figure 2. The lunar nearside DOP map of white light by our observation data. The mean spatial resolution of the DOP map is 1.58 km pixel^{-1}. The gray strip represents the zone of the Moon's terminator line during observations. The digitization of lunar mare boundaries is represented by the black solid line (Nelson et al. 2014). The typical uncertainty of the obtained DOP of white light is not larger than 0.5% for each frame by relative calibration.

locations for each sample of these missions on the DOP map. Then we averaged FeO data for each of the 15, 16, and 17 missions to compare with the DOP parameter values corresponding to their landing site. All samples averaged across the Apollo and Luna missions were used. An area of 4×4 pixels centered on each of these landing sites was averaged to determine the locations of the DOP map.

We also introduce the FeO abundances in Figure 4(b) from Kaguya Lunar Multiband Imager (MI) Derived FeO Weight Percent data (Lemelin et al. 2019) for subsequent analysis. The MI ultraviolet-visible (UV-VIS) data set, comprising five spectral bands at wavelengths of 415, 750, 900, 950, and 1001 nm, served as the foundation for generating nine fresh near-global maps illustrating the distribution of common lunar minerals, including FeO, TiO_2, and optical maturity (OMAT). These maps were derived through the application of Hapke's radiative transfer equations (Lemelin et al. 2016). However, it is important to note that the coverage of these maps is confined to latitudes within $+/-50°$. This limitation arises from the challenges encountered in accurately rectifying topographic shading at higher latitudes, as discussed by Lemelin et al. (2019).

4. Results and Discussion

We find a remarkable, linear correlation between the newly obtained DOP parameters of the lunar white light and the average FeO contents of soil samples at each site or station in

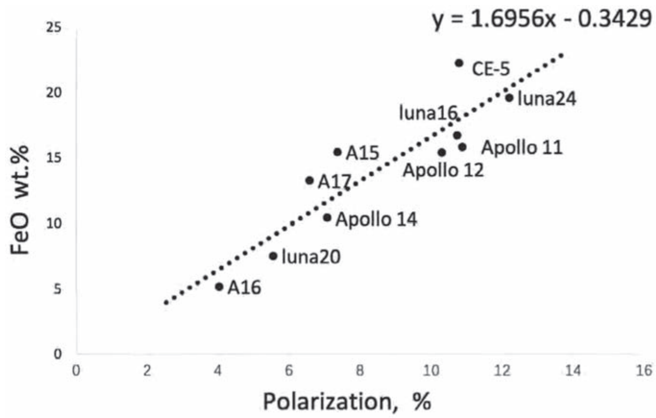

Figure 3. Graph of the average FeO contents of soils from each site or station plotted against the average polarization parameters computed from our observation data. The Pearson correlation coefficient is 0.8905. The equation of the best linear fit is shown in the figure.

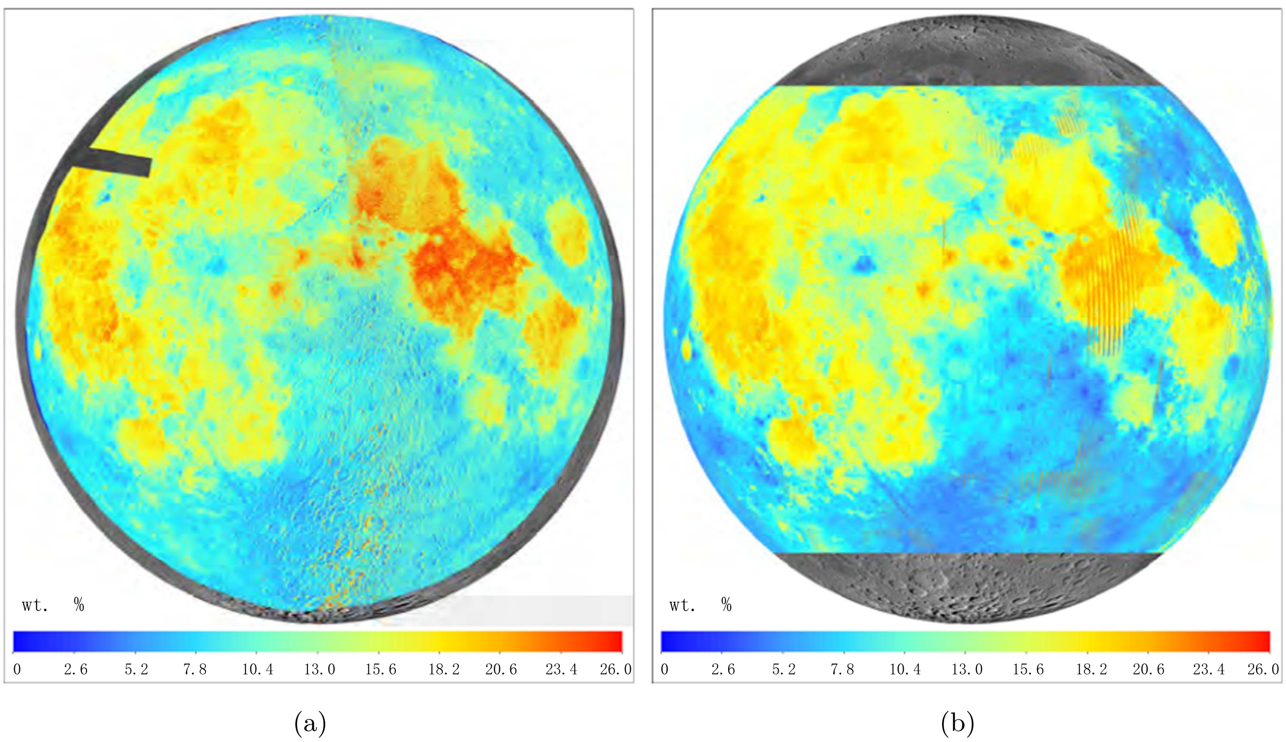

Figure 4. (a). Mapping of the FeO abundances with our polarization data using the linear fit in Figure 3. (b). Mapping of the FeO abundances with the MI UV-VIS data using Hapke's radiative transfer equations (Lemelin et al. 2016) for comparison. The background is the shaded relief map generated from Lunar Orbiter LASER Altimeter (LOLA) DEM data.

Figure 3. In addition, the present observations and analyses demonstrate that the abundance distribution of FeO on the lunar surface obtained from ground-based observations shows a significant linear relationship with the DOP, while no comparison can be made to find the association between the distribution of other materials on the lunar surface, such as TiO_2, and the white light polarization. We infer that the DOP is directly related to the abundance distribution of FeO on the lunar surface and has an exclusive relationship.

The fitted correlation equation here can be used to invert the FeO map, and a result is presented in Figure 4(a). The differences in FeO abundance results were achieved by subtracting the FeO abundances obtained from two inversion methods. The two-dimensional (2D) probability density

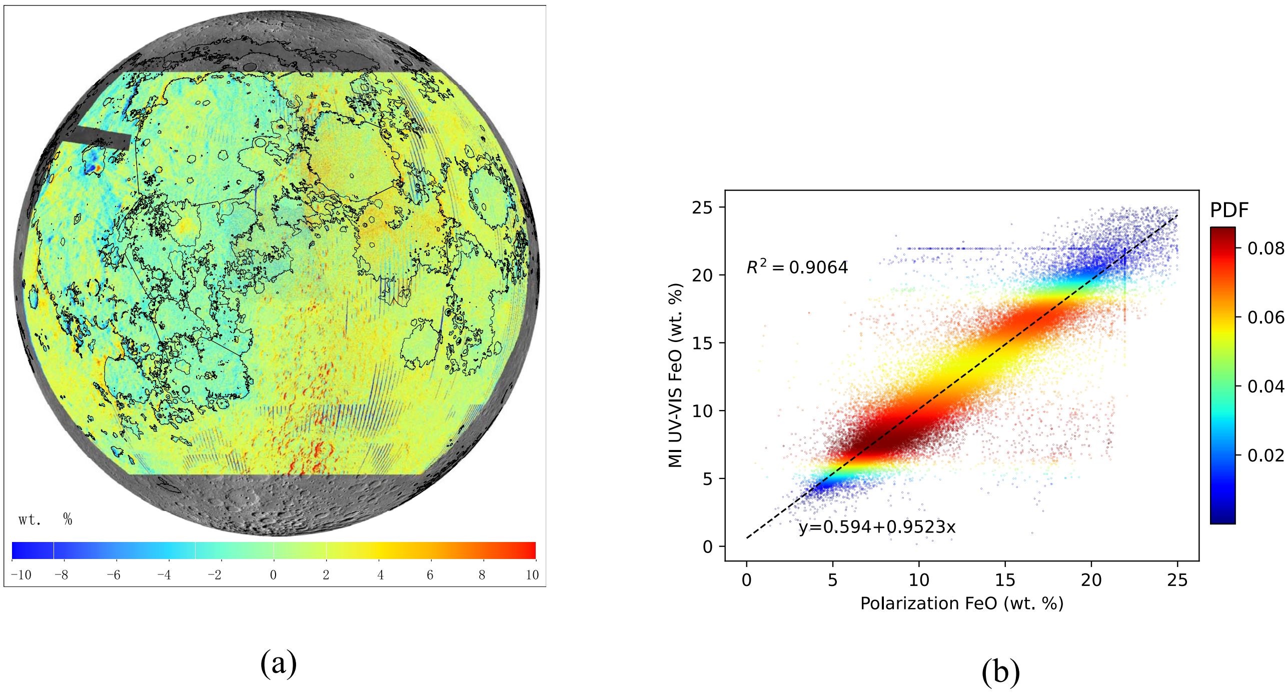

Figure 5. (a). Differences in FeO abundance are shown using the subtraction of two methods. The digitization of lunar mare boundaries is represented by the black solid line (Nelson et al. 2014). The background is the shaded relief map generated from LOLA DEM data. (b). 2D PDF scatter plots of the FeO abundances derived by this work (70°N–70°S) vs. the FeO derived from the MI UV-VIS data (Lemelin et al. 2016) and our data. MI UV-VIS data are resampled to 1.58 km $pixel^{-1}$ for comparison with our data.

Table 1
Sample-station Soil FeO Concentrations

Site	DOP (%)	FeO (wt.%)	Longitude	Latitude
Apollo11-avg (in literature)	10.87	15.8	23.47315	0.67322
Apollo12-avg (in literature)	10.29	15.4	336.5752	−3.0098
Apollo14-avg (in literature)	7.08	10.4	342.52233	−3.64408
luna16-avg (in literature)	10.72	16.7	56.3638	−0.5137
luna20-avg (in literature)	5.58	7.5	56.6242	3.7863
luna24-avg (in literature)	12.19	19.6	62.2129	12.7142
A15 average (calculated by A15-09, 9A and S1-8)	7.36	15.425	3.63803	26.13174
A16 average (calculated by A16-S1, 2, 4, 5, 8, 9, 10, 11, 13 and LM)	4.03	5.157	15.5037	−8.9729
A17 average (calculated by A17-LRV1, 2, 3, 5, 6, 7, 8, S1-S9 and LRV1-12)	6.58	13.247	30.7655	20.1923
CE-5	10.78	22.24	−51.916	43.0574

function (PDF) indicates a consistency between the FeO contents obtained from the DOP map and the MI UV-VIS data inversion in 5(b). Figure 5(a) demonstrates consistent FeO content inversions for the above two different methods in most areas of the Procellarum, but there is significant deviation in the radial pattern from the location of Aristarchus to the Promontorium Heraclides in the southwest of Sinus Iridum, as well as Kepler Crater. Furthermore, the FeO contents estimated from the DOP map exhibit significant deviations in highland regions, where the FeO content is lower. Other factors besides the FeO material composition may influence the white light polarization in highland areas.

Interestingly, impact craters near the Moon's terminator line exhibit higher polarization in Figure 2. We speculate that in those areas, the higher DOP may be caused by the larger angles of incidence of light as well as potential lunar dust transport effects (Dong et al. 2023), which consequently affect the estimation of FeO content.

The DOP map inversion results in the western hemisphere generally appear higher compared to the spectral data inversion results, as depicted in Figure 5(a). We believe that there are two factors. On the one hand, the difference is related to the material compositions from the observation and analysis results. The abundance of FeO, which produces significant polarization, is high in the western hemisphere and low on the other side. For a macroscopic level explanation, one possibility for the different polarization optical properties of different chemical substances is that it originates from the different propagation rates of left and right circularly polarized light in chiral substances, and the different polarization degrees or properties caused by the different refractive indices. From the molecular level, the different molecular electric dipole orbitals and magnetic dipole orbitals of different substances have different coupling properties, which may lead to the polarization of light across the substance crystal re-reflection of the polarization of the crystal molecules associated with the internal energy level. On the other hand, we cannot rule out that the polarization differences are also caused by the different phase angles of the Moon (the Sun-Moon-Earth geometrical configurations). These issues need to be further analyzed and studied as new topics.

5. Conclusion

Above, this study employs a novel split-focus plane polarization camera to conduct the initial white light polarization observations on the near side of the Moon. We obtained the lunar nearside DOP map of white light. The findings indicate that the white light polarization is lower in the lunar highland than maria overall. Using samples of lunar data, we noticed and determined the linear correlation between FeO abundances and white light of the DOP parameters. The white light of the DOP parameters demonstrates high consistency with FeO on the Moon. Furthermore, we estimated the lunar FeO content map by using the white light of the DOP map.

Optical polarization remote sensing contains more abundant information on physical effects compared to other optical methods, for more effective recognition of the features and physical properties of ground objects. Introducing this Earth technique into lunar study is a reasonable consideration. Ground-based lunar polarization imaging observations reflect the macroscopic and large-scale effects of lunar polarization. This study serves as an initial attempt to analyze the material composition of the lunar surface, revealing the uneven composition of the lunar surface from ground polarization imaging observations.

In the future, we will provide reference and calibration samples for similar observations by in-orbit probes, and carry out ground-based polarimetric observations of the Moon and other planetary objects in different spectral bands by using narrow-band filters to explore discoveries.

Acknowledgments

The authors thank the reviewers for their valuable comments. This work was supported by the National Key Research and Development Program of China (2021YFA0715101), partly supported by a National LLR station project, the National Natural Science Foundation of China (NSFC, Grant Nos. 11973064 and 42101413), Jilin Province Mid-youth science and technology innovation and entrepreneurship outstanding talent project (20220508147RC) and the Changchun City and Chinese Academy of Sciences Science and Technology Cooperation High-tech Industrialization Special Fund Project (21SH05).

ORCID iDs

Wei-Nan Wang https://orcid.org/0009-0008-7164-4440

References

Blewett, D. T., Lucey, P. G., Hawke, B. R., & Jolliff, B. L. 1997, JGR, 102, 16319
Dollfus, A., & Titulaer, C. 1971, A&A, 12, 199
Dong, T., Yulong, F., Wei, H., et al. 2023, J. Tsinghua Univ. (Sci. Technol.), 63, 433
Fearnside, A., Masding, P., & Hooker, C. 2016, Icar, 268, 171
Gao, S., & Gruev, V. 2011, OExpr, 19, 26161
Gillis, J. J., Jolliff, B. L., & Elphic, R. C. 2003, JGRE, 108, 5009
Heiles, C. 2000, AJ, 119, 923
Jeong, M., Kim, S. S., Garrick-Bethell, I., et al. 2015, ApJS, 221, 16
Lemelin, M., Lucey, P. G., Gaddis, L. R., Hare, T., & Ohtake, M. 2016, in 47th Lunar and Planetary Science Conference
Lemelin, M., Lucey, P. G., Miljkovi, K., et al. 2019, P&SS, 165, 243
Li, C., Hu, H., Yang, M.-F., et al. 2021, Natl Sci. Rev., 9, nwab188
Lucey, P. G., Blewett, D. T., & Hawke, B. R. 1998, JGRE, 103, 3679
Nelson, D., Koeber, S., Daud, K., et al. 2014, in 45th Lunar and Planetary Science Conf., 2861
Powell, S. B., & Gruev, V. 2013, OExpr, 21, 21039
Ramaprakash, A. N., Rajarshi, C. V., Das, H. K., et al. 2019, MNRAS, 485, 2355
Ratliff, B. M., LaCasse, C. F., & Tyo, J. S. 2009, OExpr, 17, 9112
Shkuratov, Y., Kaydash, V., Korokhin, V., et al. 2011, P&SS, 59, 1326
Shkuratov, Y., & Opanasenko, N. 1992, Icar, 99, 468
Shkuratov, Y. G. 1981, SvA, 25, 490
Sim, C. K., Kim, S. S., Jeong, M., Choi, Y.-J., & Shkuratov, Y. G. 2019, PASP, 132, 015004
Słowikowska, A., Krzeszowski, K., Żejmo, M., Reig, P., & Steele, I. 2016, MNRAS, 458, 759
Turnshek, D. A., Bohlin, R. C., Williamson, R. L. I., et al. 1990, AJ, 99, 1243
Tyo, J. S., Goldstein, D. L., Chenault, D. B., & Shaw, J. A. 2006, ApOpt, 45, 5453